 https://doi.org/10.3311/PPch.42159

Periodica Polytechnica Chemical Engineering, 70(2), pp. 344–356, 2026

Properties of Hyaluronic Acid–Polyvinylpyrrolidone Blends as Green Plastic Materials

Budiman Anwar[1*], Gabriela Chelvina Santiuly Girsang[1], Soja Siti Fatimah[1], Iqbal Musthapa[2], Fitri Khoerunnisa[3]

[1] ChemTransform for Sustainability Research Group, Chemistry Programs, Faculty of Mathematics and Natural Science Education, Universitas Pendidikan Indonesia, Jl. Dr. Setiabudi 229, Bandung 40154-Indonesia
[2] BioCoFA Research Group, Chemistry Programs, Faculty of Mathematics and Natural Science Education, Universitas Pendidikan Indonesia, Jl. Dr. Setiabudi 229, Bandung 40154-Indonesia
[3] Environmental Chemistry Research Group, Chemistry Programs, Faculty of Mathematics and Natural Science Education, Universitas Pendidikan Indonesia, Jl. Dr. Setiabudi 229, Bandung 40154-Indonesia
* Corresponding author, e-mail: budimananwar@upi.edu

Received: 08 September 2025, Accepted: 10 March 2026, Published online: 28 April 2026

Abstract

Hyaluronic acid (HA) and polyvinylpyrrolidone (PVP) have garnered considerable attention as components in biodegradable films and bioplastics due to their favorable physicochemical properties and biocompatibility. HA is known for its natural origin, biodegradability, and excellent biocompatibility, while PVP is valued for its outstanding film-forming ability, water solubility and non-toxic nature, making both polymers promising candidates for environmentally friendly and biomedical polymer systems. Investigating the combination of these two polymers may therefore provide findings of significant scientific relevance. This study investigates the influence of HA and PVP composition on the structural and physicochemical properties of their polymer blend films. Scanning electron microscopy and differential scanning calorimetry (DSC) analyses demonstrated excellent compatibility and miscibility between HA and PVP. Fourier transform infrared spectroscopy indicates that the incorporation of PVP disrupts the intermolecular hydrogen bonding within HA matrix. Furthermore, SEM and X-ray diffraction analyses reveal that increasing the PVP content enhances morphological uniformity and crystallinity, respectively. Correspondingly, the mechanical properties of the films improve with higher PVP content. At an HA/PVP ratio of 1:7 (w/w), the films exhibit a tensile strength of 49.93 ± 9.34 MPa, an elongation at break of 6.89 ± 0.31% and an elastic modulus of 1.06 ± 0.24 GPa. The incorporation of PVP leads to lower film transparency, a higher water vapor transmission rate, and decreased surface wettability. Thermal analysis by thermogravimetric analysis and DSC indicates that the incorporation of PVP improves the thermal stability while simultaneously lowering the glass transition temperature.

Keywords

hyaluronic acid, polyvinylpyrrolidone, polyblend, biodegradable plastics, biopolymers

1 Introduction

Plastics are essential to modern life but contribute significantly to climate change and global pollution due to energy-intensive production processes and waste management challenges [1]. With the rapid progress of industry and economic development, plastic pollution has become a defining characteristic of modern society, with plastic debris and microplastics now detected across virtually all environmental compartments, including oceans, soil, air, rainwater, remote ecosystems, and even the human body [2]. Among various forms of plastic pollution, microplastics – plastic particles smaller than 5 mm – have emerged as a particularly critical concern due to their high environmental persistence, fragmentation potential, and ability to adsorb and transport other pollutants [3]. These microplastic particles are frequently ingested by marine organisms across multiple trophic levels, where their physicochemical properties enable the adsorption of environmental contaminants, facilitating contaminant transfer within food webs and potentially leading to physical harm and toxicological effects [4]. In agricultural systems, while plastic products contribute to improved crop yield, water efficiency, and food quality, their extensive use has also led

Cite this article as: Anwar, B., Girsang, G. C. S., Fatimah, S. S., Musthapa, I., Khoerunnisa, F. "Properties of Hyaluronic Acid–Polyvinylpyrrolidone Blends as Green Plastic Materials", Periodica Polytechnica Chemical Engineering, 70(2), pp. 344–356, 2026. https://doi.org/10.3311/PPch.42159

to significant contamination of soil, water and plants, posing risks to ecosystems and long-term food security [5]. These findings indicate that plastic pollution poses risks to environmental and human health and may hinder progress toward global sustainability targets, highlighting the need to develop biodegradable and environmentally safer alternatives to conventional plastics.

To address these issues, the use of biodegradable materials as alternatives to conventional plastics in packaging and other applications has been increasingly explored. Polysaccharides, in particular, are widely utilized in the development of films, coatings and aerogels for food packaging, and related uses owing to their abundance, sustainability, biocompatibility and biodegradability [6].

Hyaluronic acid (HA), a natural polysaccharide polymer, is being explored as a promising material for plastic film applications [7]. HA films exhibit a uniform structure and outstanding tensile strength, ranging from 10 to 80 MPa [8, 9], significantly higher than that of other polysaccharide-based films such as starch, chitosan, and pectin [10]. In addition, HA films demonstrate high transparency, reaching up to 90% [11], which makes them visually attractive for packaging applications. However, despite these advantages, HA films are limited by poor thermal stability and higher raw material costs compared to other natural polysaccharides. To overcome these challenges, this study utilizes a polymer blending approach by incorporating polyvinylpyrrolidone (PVP) into the HA matrix [12].

PVP was selected as the blending material not only due to its cost-effectiveness, but also because of its excellent miscibility in aqueous solvent systems. Previous studies have demonstrated the successful incorporation of PVP into biopolymers such as chitosan [11], hydroxyethylcellulose (HEC) [13], hydroxypropylmethylcellulose (HPMC) [14], and ethylcellulose (EC) [15]. The addition of PVP has been reported to improve film morphology, yielding transparent, uniform, and defect-free structures [13, 16]. Furthermore, in polymer blends, PVP is frequently employed to enhance thermal stability due to its high decomposition temperature, which can reach up to 400 °C [17].

Although water-soluble polymers are often perceived as unsuitable for packaging applications, they offer unique advantages for specific and emerging packaging concepts rather than conventional long-term moisture-barrier packaging. Water-soluble and biodegradable polymer films have been widely explored as edible or dissolvable packaging materials, such as single-use sachets for food seasonings, instant beverages, or pharmaceutical doses, which can be directly dissolved in water during use, thereby eliminating post-consumer plastic waste [18]. In this context, hydrophilicity and controlled solubility become functional attributes rather than limitations. Furthermore, polymers such as HA and PVP exhibit excellent film-forming ability, biocompatibility, and tunable physicochemical properties, enabling their use not only in packaging but also in advanced functional applications, including polymer electrolyte membranes [19, 20], biomedical films [21, 22], and biodegradable coatings [23, 24]. Given the complementary properties of HA and PVP, combining both polymers into a single blend is expected to integrate their film-forming capability, biocompatibility, and tunable physicochemical characteristics, making HA/PVP films promising candidates for sustainable and application-oriented polymer systems.

Lewandowska and Szulc [25] investigated the miscibility of HA and PVP mixtures, as well as the intermolecular interactions between the two polymers. Their results showed that miscible HA/PVP blends are formed when the PVP content exceeds that of HA. Blending HA with PVP provides a promising route for developing novel materials by combining the distinct physicochemical properties of each polymer. However, to date, no studies have specifically examined HA/PVP blend films with respect to the effects of composition on their structural, morphological, mechanical, thermal, optical, and water vapor barrier properties. Therefore, the present study aims to investigate how the HA/PVP composition influences the structure and physicochemical characteristics of the resulting polymer blend films.

In this study, HA/PVP blend films were prepared using the solution casting method. The structural characteristics were examined in terms of morphology, functional group shifts, and crystallinity using scanning electron microscopy (SEM), Fourier transform infrared spectroscopy (FTIR) and X-ray diffraction (XRD), respectively. The physicochemical properties of the films were evaluated with respect to their mechanical, thermal, optical and water vapor barrier performance. Thermal analysis included the assessment of thermal degradation and key thermal parameters such as glass transition temperature, melting temperature, crystallization temperature, and their corresponding enthalpy values. Furthermore, in applications such as packaging films or polymer electrolyte membranes, a thorough understanding of these physicochemical properties is crucial for designing suitable compositions and evaluating their performance under diverse conditions.

2 Material and methods

2.1 Materials

HA powder (cosmetic grade, high molecular mass, 1500 kDa) and PVP K-30 powder (pharmaceutical grade, 40 kDa) were purchased from Interco Laboratories, Bandung, Indonesia. All other reagents were of analytical grade and obtained from commercial sources (Merck and Sigma-Aldrich).

2.2 Preparation of HA/PVP blend films

The HA/PVP composition was varied at different weight ratios of HA to PVP, i.e. 1:1, 1:3, and 1:7 (w/w), as presented in Table 1. The selection of this composition is based on the findings of Lewandowska and Szulc [25], which reported that miscible HA/PVP blends are formed when the PVP content exceeds that of HA. HA powder was dissolved in 70 mL of distilled water, while PVP powder was dissolved separately in 30 mL of distilled water. The PVP solution was then added to the HA solution and stirred without heating for 2.5 h using a magnetic stirrer. The resulting HA/PVP mixture was degassed in an ultrasonic bath for 30 min to remove air bubbles. Subsequently, 30 mL of the mixture was poured into acrylic Petri dishes and allowed to dry at room temperature. After drying, the films were carefully peeled off and stored in a desiccator for 72 h to prevent moisture absorption. Pure HA and PVP films were also prepared using the same procedure for comparison.

2.3 Characterization of HA/PVP films

SEM analysis was conducted on both the surface and cross-section of the films using an FEI Quanta 450 instrument (FEI Company, Hillsboro, USA) operated at 15 kV to examine film morphology. Surface images were captured at 1000x magnification, while cross-sectional images were acquired at 1000x, 2000x, 5000x, and 10,000x magnifications. The resulting SEM images were processed and analyzed using ImageJ software.

FTIR analysis was performed on the film samples using an Alpha II spectrometer (Bruker, Ettlingen, Germany) to identify changes in chemical composition and intermolecular interactions, particularly hydrogen bonding. FTIR spectra were recorded in the range of 4000–400 cm^{-1} at a resolution of 4 cm^{-1}. To further evaluate hydrogen bonding, the hydrogen bond energy (E_H) and hydrogen bond length (R) were calculated using Eqs. (1) and (2), respectively [13, 26].

$$E_H = \frac{1}{k}\left[\frac{v_0 - v}{v_0}\right] \tag{1}$$

where v_0 is the standard frequency (which refers to the characteristic wavenumber of free (non-hydrogen-bond) OH groups, tipically observed around ~3600 cm^{-1}), v is the frequency of the bonded OH, and k is a constant ($1/k = 2.626 \times 102$ kJ/mol)

$$\Delta v\left(\mathrm{cm}^{-1}\right) = 4430\left(2.84 - R\right) \tag{2}$$

where $\Delta v = v_0 - v$, v_0 is the frequency of monomeric OH stretching (3600 cm^{-1}) and v is the stretching frequency observed in the infrared spectra of the samples.

XRD analysis was conducted to investigate the crystallinity index (CI) and crystallite size (L) of the films. Characterization was performed at room temperature using a MiniFlex diffractometer (Rigaku, Tokyo, Japan) equipped with a CuKα radiation source (λ = 0.154 nm), operating over a 2θ range of 2–90°, with a scan step of 0.02°, a generator voltage of 45 kV, and a tube current of 40 mA. The crystallite size was calculated using the Scherrer equation [27], as shown in Eq. (3):

$$D = \frac{K \times \lambda}{H \times \cos\theta} \tag{3}$$

where K is the Scherrer constant (0.94), λ is the X-ray wavelength (0.154 nm), H is the full width at half maximum (FWHM) in radians, and θ is the Bragg angle. The crystallinity index of the films was calculated as the ratio of the crystalline diffraction area (A_c) to the total diffraction area, as shown in Eq. (4).

$$CI\left(\%\right) = \frac{A_c}{\text{Total area}} \times 100\% \tag{4}$$

The mechanical properties, including tensile strength, elongation at break and Young's modulus, were evaluated using a Textechno Favigraph I-PI-067 instrument (Textechno H. Stein GmbH & Co. KG, Mönchengladbach, Germany) at a crosshead speed of 6.0 mm/min under dry conditions at room temperature. All film samples were uniformly cut to dimensions of 3 mm × 50 mm.

The water vapor transmission rate ($WVTR$) test was conducted using a modified method based on previously reported research [28]. In this procedure, a film sample was

Table 1 HA/PVP films compositions

No	Sample	HA/PVP ratio	HA [mg]	PVP [mg]	Water [mL]
1	HA/PVP1	1:1	1000	1000	100
2	HA/PVP3	1:3	500	1500	100
3	HA/PVP7	1:7	250	1750	100
4	Pure HA	1:0	2000	-	100
5	Pure PVP	0:1	-	2000	100

secured over the opening of a glass vial containing 5 g silica gel, ensuring complete coverage. The vial was placed in a sealed plastic container with a rubber-lined lid, containing distilled water at a depth of approximately 3 cm. The container was kept undisturbed for 24 h. After this period, the silica gel was reweighed, and the *WVTR* was calculated using Eq. (5).

$$WVTR = \frac{\Delta W}{A \times t} \tag{5}$$

where ΔW is the difference between the initial and final mass (g), A is the surface area of the film (m^2), and t is the storage time (days).

A laboratory-scale contact angle measurement setup was employed to evaluate the surface wettability of the film samples. Film specimens with dimensions 10 mm × 10 mm were placed on a horizontal sample stage, and a droplet of distilled water was carefully deposited onto the film surface using a syringe. The shape of the water droplet formed on the film surface was recorded using a digital camera for subsequent contact angle analysis [13].

Film samples measuring 4.3 cm × 0.9 cm were placed in a transparent cuvette, and their absorbance was measured using a UVmini-1240 UV-Vis spectrophotometer (Shimadzu, Kyoto, Japan), with air as the blank, to determine the light transmission and opacity of the films [29]. The opacity was calculated using Eq. (6), where A_{600} represents the absorbance at a wavelength of 600 nm, and l is the film thickness (mm).

$$\text{Opacity} = \frac{A_{600}}{l} \tag{6}$$

The thermal properties of the films were analyzed using a TGA701 thermogravimetric analyzer (LECO, St. Joseph, MI, USA) and a DSC 214 Polyma (Netzsch, Selb, Germany). For thermogravimetric analysis (TGA), film samples with known masses were heated from 25 °C to 600 °C at a rate of 5 °C/min under a nitrogen atmosphere. For differential scanning calorimetry (DSC), the film samples were hermetically sealed in DSC pans and heated from 25 °C to 250 °C at a rate of 10 °C/min, also under a nitrogen atmosphere. The sample mass used in the analysis ranged between 5.90 and 7.10 mg.

3 Result and discussion

3.1 Morphology of the films

Fig. 1 shows photographs of the blend films with different compositions of HA and PVP. All films appear transparent.

The incorporation of PVP led to changes in the surface morphology (Fig. 2) and cross-sectional structure (Fig. 3) of the films. The pure HA film exhibited a dense structure with a smooth surface and cross-section. Upon the addition of PVP in the HA/PVP1 film, surface indentations appeared, and clumps were observed in the cross-section.

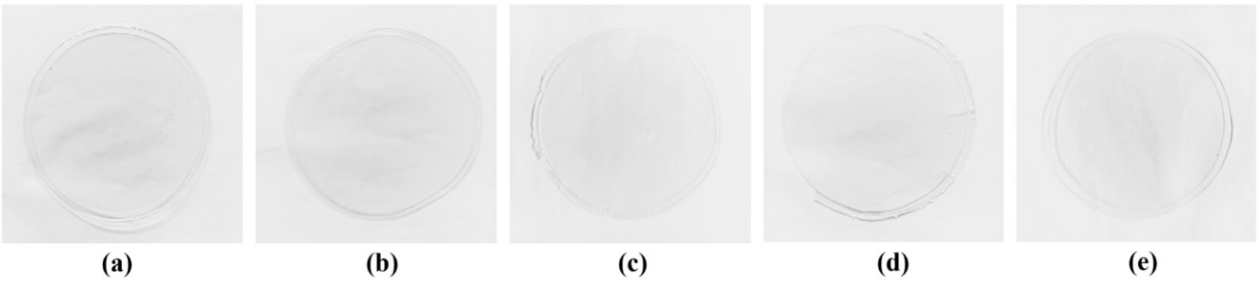

Fig. 1 Photograph of (a) HA, (b) PVP, (c) HA/PVP1, (d) HA/PVP3 and (e) HA/PVP7 films

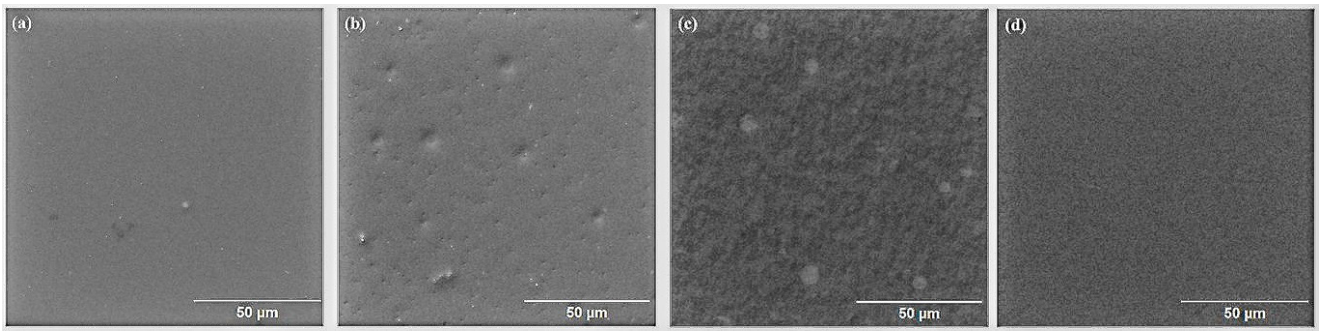

Fig. 2 Surface morphology of (a) HA, (b) HA/PVP1, (c) HA/PVP3 and (d) HA/PVP7 films at 1000x magnification

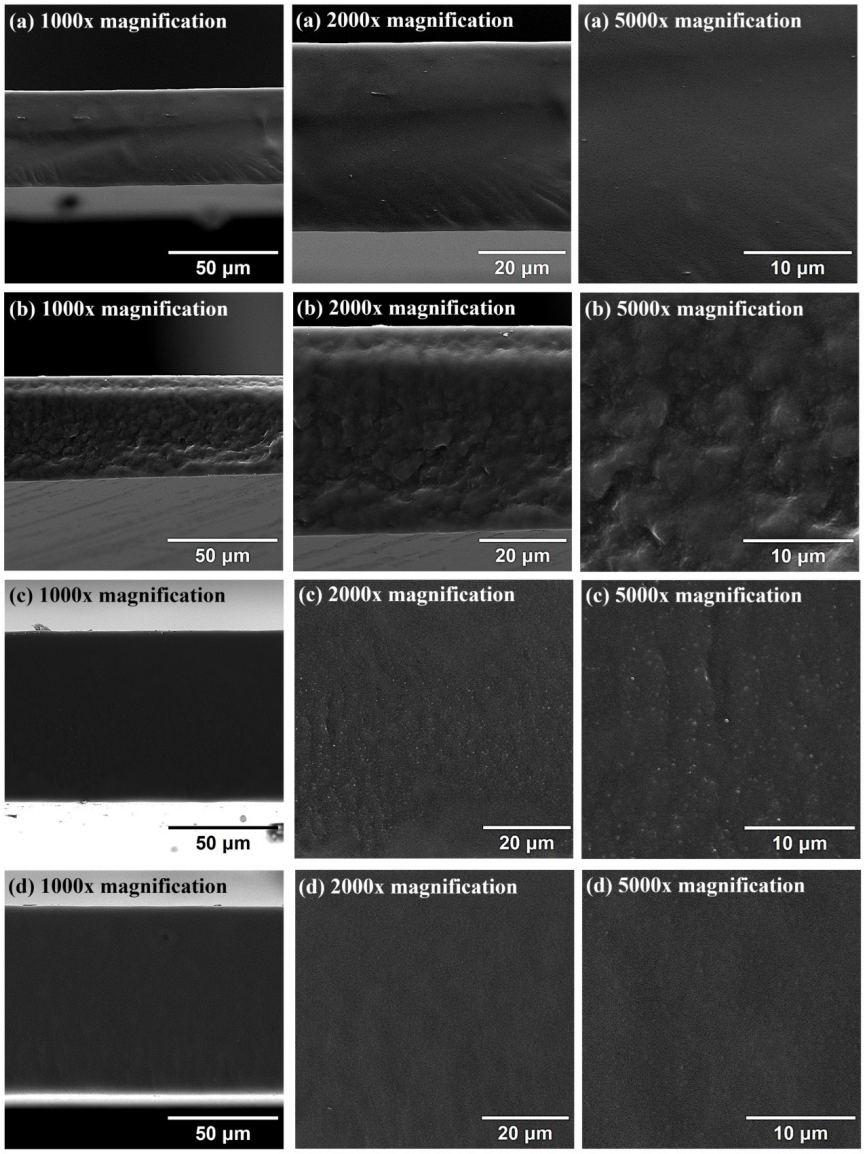

Fig. 3 Cross-sectional morphology of (a) HA, (b) HA/PVP1, (c) HA/PVP3 and (d) HA/PVP7 films, shown at magnifications of 1000x, 2000x and 5000x from left to right

These clumps and irregularities suggest poor miscibility between HA and PVP at this composition.

An increase in PVP content, as seen in the HA/PVP3 and HA/PVP7 films, resulted in a morphological transition from heterogeneous to homogeneous and defect-free. Compared with HA/PVP3, the HA/PVP7 film exhibited enhanced surface uniformity, although it did not reach the level of homogeneity observed for the neat HA film. Its cross-section showed minimal texture and appeared smoother, indicating excellent miscibility and compatibility between HA and PVP at this ratio. These results are in agreement with the findings reported by Lewandowska and Szulc [25].

As the PVP content increased, as observed in the HA/PVP3 and HA/PVP7 films, the morphology transitioned from heterogeneous to homogeneous and defect-free. Among these, the HA/PVP7 film exhibited greater uniformity than HA/PVP3. Its cross-section showed minimal texture and appeared smoother, indicating excellent miscibility and compatibility between HA and PVP at this ratio.

3.2 XRD analysis

Fig. 4 presents the XRD diffractograms of HA, PVP and HA/PVP blend films. The corresponding peak positions, crystallinity index, and crystallite size are summarized in Table 2. All films exhibit two broad diffraction peaks at approximately $2\theta = 11°$ and 20°. These broad peaks indicate the predominantly amorphous nature of the polymer

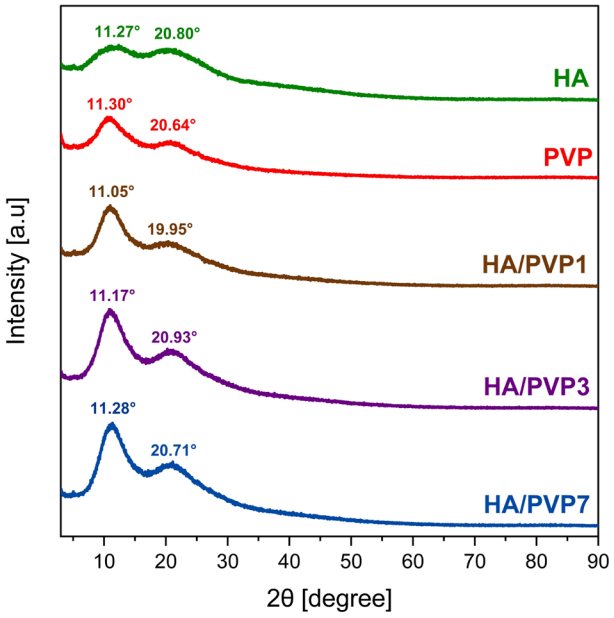

Fig. 4 XRD diffractograms of HA, PVP and HA/PVP blend films

Table 2 Crystallite size and crystallinity index of the HA, PVP and HA/PVP blend films

Sample	2θ [degree]	FWHM [degree]	*L* [nm]	*CI* [%]
HA	11.27 20.80	5.78 11.08	1.05	27
PVP	11.30 20.64	4.61 11.06	1.23	41
HA/PVP1	11.05 19.95	4.32 11.81	1.26	34
HA/PVP3	11.17 20.93	4.69 11.42	1.20	42
HA/PVP7	11.28 20.71	4.57 11.89	1.21	44

films. Generally, polymeric materials do not form long-range crystalline structures and thus display amorphous or semicrystalline diffraction patterns within the 2θ range of 10°–25° [30].

The HA film exhibited a more amorphous profile than PVP, as evidenced by its lower *CI* of 27%. This amorphous nature can be attributed to the absence of long-range molecular order, likely resulting from the intercalation and random orientation of HA polymer chains. The XRD pattern of the HA film observed in this study is consistent with that reported for high-molecular-weight HA films in a previous study [31].

The blending of HA with PVP generated an X-ray diffraction pattern that differed from those of the individual HA and PVP films. The incorporation of PVP resulted in increased peak intensity and crystallinity index values, suggesting the formation of a more ordered polymer chain arrangement. In contrast to previous studies that reported PVP promotes amorphous structure formation in biopolymer/PVP films [32, 13], the present findings indicate that PVP can serve as a nucleation site within the polymer matrix. PVP has previously been shown to facilitate crystal formation and growth, as in the case of naproxen crystals [33]. Its linear structure and substantially lower molecular weight compared to HA enable it to intercalate into the HA polymer network during blending, thereby contributing to the formation of a new crystalline phase. Additionally, the observed shift in 2θ values suggests alterations in the crystal lattice parameters induced by PVP incorporation.

In polymer blend films, the distribution and size of crystallites significantly influence the microstructure and homogeneity of the film. In this study, variations in crystallite size correlate with cross-sectional morphological features observed in the SEM analysis. The HA/PVP1 film exhibited the largest crystallite size (1.26 nm), likely due to phase separation, which was evident as clump formations in the film's cross-section (Fig. 3(b)). As the PVP concentration increased in the HA/PVP3 and HA/PVP7 films, the crystallite size decreased (1.20–1.21 nm). This reduction can be attributed to the development of a more uniform morphology, facilitated by the formation of new crystalline structures where PVP acts as nucleation sites, resulting in the formation of smaller crystals. Similar trends were reported in a study on polycaprolactone (PCL) blended with oxidized starch [34].

3.3 Mechanical properties

The mechanical properties of HA, PVP and HA/PVP blend films are summarized in Table 3, while the corresponding stress-strain curves are presented in Fig. 5. The stress-strain curves represent the results obtained from three repeated tensile measurements, and the mechanical parameters listed in Table 3 are reported as the average values derived from these measurements. These properties are influenced by intermolecular forces, crystallinity, polymer

Table 3 Mechanical properties of HA, PVP and HA/PVP blend films

Sample	Tensile strength [MPa]	Elongation at break [%]	Young's modulus [GPa]
HA	65.71 ± 3.91	41.26 ± 6.79	1.11 ± 0.44
PVP	62.00 ±16.90	7.85 ± 1.40	1.04 ± 0.10
HA/PVP1	40.85 ± 7.69	5.62 ± 0.76	1.11 ± 0.14
HA/PVP3	41.72 ± 7.75	5.40 ± 0.43	1.10 ± 0.17
HA/PVP7	49.93 ± 9.34	6.89 ± 0.31	1.06 ± 0.24

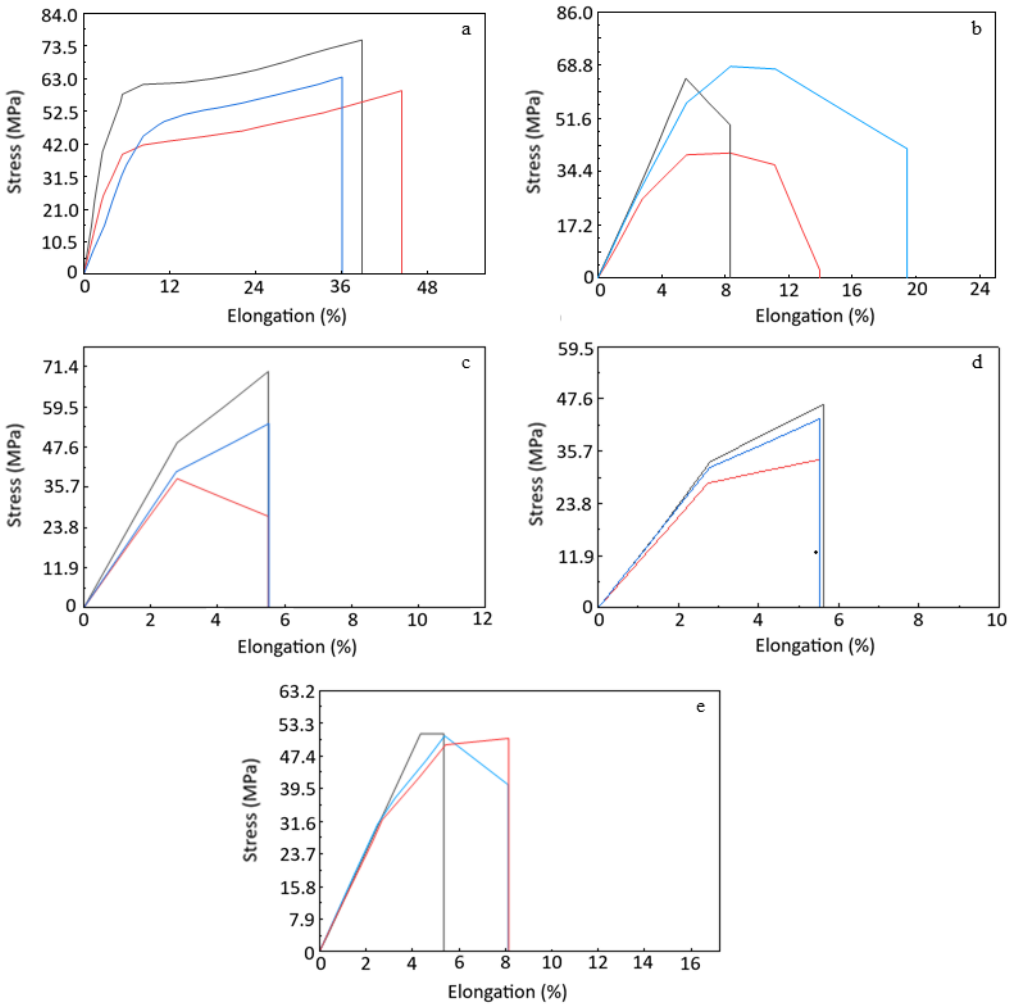

Fig. 5 Stress-strain curves of (a) HA, (b) PVP, (c) HA/PVP1, (d) HA/PVP3 and (e) HA/PVP7

molecular weight, and film morphology. The strong intermolecular hydrogen bonding between polymer chains in the HA film results in higher tensile strength [32, 35]. Furthermore, the homogeneous morphology and absence of cavities or defects in the HA film minimize crack initiation sites and facilitate more efficient stress distribution [36]. These observations are supported by SEM, FTIR and DSC analyses. Additionally, the enhanced plastic deformation capacity, as indicated by the high elongation at break, can be attributed to the low crystallinity of the HA film. In semi-crystalline polymers, the amorphous regions are more capable of undergoing deformation [37]. This finding is also supported by XRD analysis.

Overall, the three blend films (HA/PVP1, HA/PVP3 and HA/PVP7) exhibit lower tensile strength and elongation at break compared to the HA film, while the Young's modulus remains relatively unchanged. The decline in tensile strength can be attributed to weakened intermolecular forces. Compared to the HA film, the HA/PVP7 blend film showed weaker intermolecular interactions, which will be elaborated further in the FTIR analysis section. In contrast, the reduction in elongation at break can be attributed to the increase in crystallinity, as evidenced by XRD analysis.

When comparing HA/PVP films with varying compositions, increasing the PVP content leads to higher tensile strength. In this trend, crystallinity and film morphology play a more significant role in determining the mechanical properties of the films. At an HA/PVP ratio of 1:7 (w/w), the films exhibit mechanical properties comparable to those of poly(lactic acid) (PLA) and poly(vinyl alcohol) (PVA), with a tensile strength of 49.93 ± 9.34 MPa, an elongation at break of 6.89 ± 0.31%, and an elastic modulus of 1.06 ± 0.24 GPa.

3.4 FTIR analysis

The FTIR spectra of HA, PVP and HA/PVP films are presented in Fig. 6, with the identified functional groups and their corresponding peak wavenumbers summarized in Table 4 [27, 38–40]. Characteristic peaks of both HA

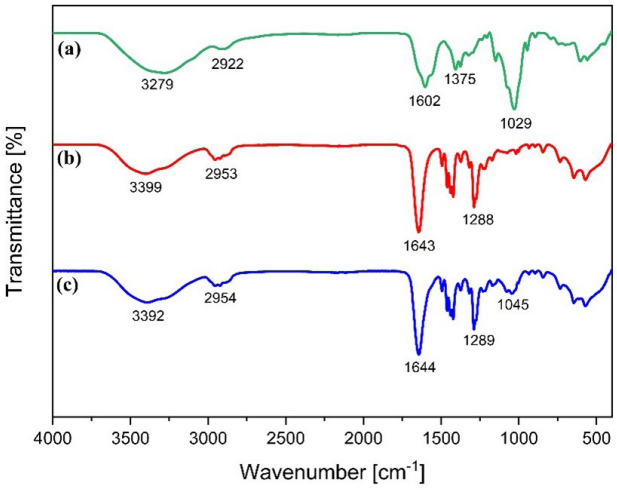

Fig. 6 FTIR spectra of (a) HA, (b) PVP and (c) HA/PVP7 films

Table 4 Characteristic infrared absorption peak of HA, PVP and HA/PVP7 films [27, 38–40]

Bond types	Modes	Wavenumber [cm^{-1}]		
		HA	PVP	HA/PVP7
−OH	Stretching	3279	3399	3392
−CH_2	-	2922	2953	2954, 2922
COO−	Symmetric	1602	-	-
COO−	Asymmetric	1406	-	-
C−O−C hemiacetal		1029	-	1045
C=N	-	-	1643	1644
C−N	-	-	1494	1494
C−H	Bending	-	1461	1462
CH_2	Wagging	-	1422	1422
C−H	-	1375	1373	1374
CH_2	Symmetric twisting	-	1288, 1218	1289, 1229
C−C	Stretching	-	1171, 844, 733	1168, 844, 733
C=O	Stretching	-	-	-
C−O	Stretching	-	-	-
C−O	Stretching	-	-	-

and PVP are present in the FTIR spectrum of the HA/PVP film, with no new peaks observed. Shifts in the -OH and C=O absorption bands indicate that HA and PVP interact through hydrogen bonding. Additionally, a shift in the C-O-C hemiacetal functional group of HA suggests a change in the molecular conformation of the HA polymer chain as a result of blending with PVP.

Further analysis of hydrogen bonding interactions in each film was conducted by evaluating the hydrogen bond energy (E_H), as presented in Table 5. The HA film exhibited the highest hydrogen bond energy and the shortest hydrogen bond distance, indicating strong intermolecular hydrogen bonding between polymer chains. The incorporation of PVP weakened these interactions, as evidenced by a decrease in hydrogen bond energy. This result support the mechanical characteristics of the HA/PVP7 film, with a notable effect on its tensile strength.

3.5 Barrier properties

Incorporation of PVP into the HA matrix led to an increase in *WVTR*; however, the values remained lower than those of the PVP film, as shown in Table 6. These results indicate that the hydrophilic nature and the relative PVP content significantly affect the *WVTR*. As PVP possesses strong affinity for water molecules, its incorporation increases the free volume and enhances water vapor diffusion across the film. This trend is in agreement with previous findings [41], which also reported that higher PVP fractions promote greater permeability due to its hydrophilic character. Nevertheless, the HA/PVP7 blend film demonstrates superior barrier properties compared to the HEC/PVP film described in earlier studies [13].

3.6 Contact angle measurement

The surface wettability of the films was evaluated through water contact angle measurements to gain insight into their surface characteristics. The neat HA film exhibited a contact angle of 60.7°, indicating a relatively hydrophilic surface [42]. Upon incorporation of PVP, the HA/PVP7 blend film showed a slightly higher contact angle of 66.0°, suggesting a moderate reduction in surface wettability compared to the pure HA film. The contact angle of HA film and HA/PVP7 blend film are shown in Fig. 7.

The higher contact angle observed for HA/PVP7 correlates well with its increased *WVTR* relative to HA.

Table 5 Hydrogen bond energy and hydrogen bond length of HA, PVP, and HA/PVP7 films

Sample	E_H [kJ/mol]	R (Å)
HA	26.61	2.768
PVP	17.99	2.795
HA/PVP7	18.52	2.793

Table 6 *WVTR* value of HA, PVP and HA/PVP blend films

Sample	*WVTR* [g/m^2 × h]	Normalized WVTR [g.mm/m^2 × h]
HA	32.67 ± 1.11	2.05 ± 0.05
PVP	75.07 ± 2.47	6.98 ± 0.26
HA/PVP7	69.12 ± 1.14	5.76 ± 0.38

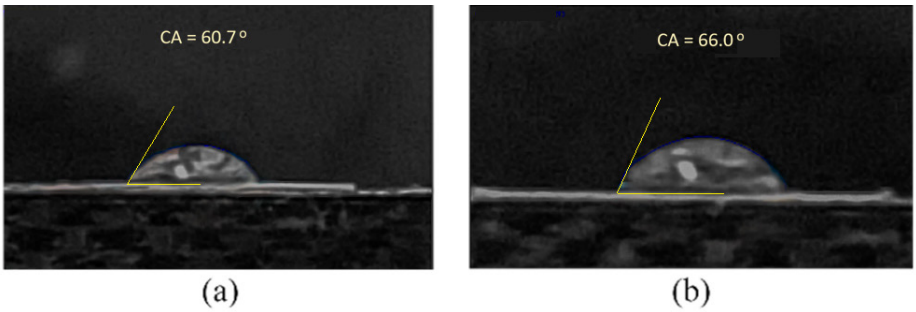

Fig. 7 Contact angle of (a) HA film and (b) HA/PVP7 blend film

Although PVP is intrinsically hydrophilic, its incorporation into the HA matrix alters the surface structure and polymer chain arrangement, which can reduce the availability of hydrophilic functional groups at the film–air interface. Consequently, the HA/PVP7 film exhibits a less wettable surface while allowing higher water vapor permeation through the bulk of the film, as reflected by the increased *WVTR* [43].

Surface morphology also plays an important role in the observed wettability behavior. SEM analysis revealed that the neat HA film possesses a more homogeneous and smoother surface compared to the HA/PVP7 blend film, which exhibits increased surface heterogeneity. Such morphological differences can influence contact angle measurements, as smoother and more uniform surfaces generally promote better wetting, whereas surface irregularities may lead to increased apparent contact angles [25].

3.7 Optical properties

One of the important factors that should be examined in the manufacture of plastic packaging is its optical properties [44]. The opacity values of HA and HA/PVP7 films are presented in Table 7.

The incorporation of PVP into HA increases the film's opacity, indicating a reduction in transparency. This reduction is attributed to light scattering caused by crystalline regions within the HA/PVP7 film, as confirmed by the XRD analysis. As more light is scattered, less is able to penetrate the film. This scattering disrupts the light transmission pathway, rendering the film less transparent. Nonetheless, the HA/PVP7 blend film exhibits considerably higher transparency compared to the HEC/PVP film reported in previous studies [13].

Table 7 Opacity of HA and HA/PVP films

Sample	Film thickness (mm)	Absorbance at 600 nm	Opacity (1/mm)
HA	0.06	0.042	0.70
HA/PVP7	0.08	0.058	0.73

3.8 Themal properties

The DSC thermograms of HA, PVP, and HA/PVP7 blend films are showed in Fig. 8 and the thermal poperties of the samples are presented in Table 8. The neat HA film exhibits a glass transition temperature (T_g) at a higher temperature with a greater relaxation enthalpy (ΔH_{relax}) than the PVP film, which can be attributed to the stronger intermolecular interactions and higher molecular weight of HA, requiring higher energy to induce chain mobility.

For the HA/PVP7 blend film, only a single T_g is observed, with a transition profile distinct from those of the individual HA and PVP films. The presence of a single, composition-dependent T_g provides clear evidence of good miscibility and compatibility between HA and PVP at this blend ratio. The incorporation of PVP into the HA matrix

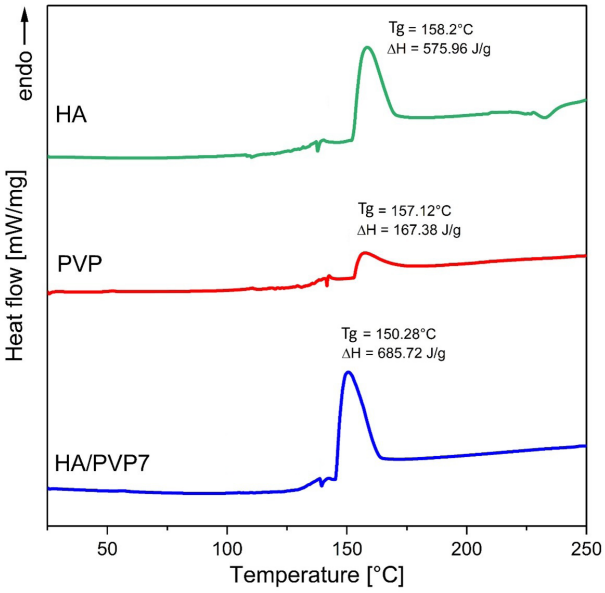

Fig. 8 DSC thermograms of HA, PVP, and HA/PVP films

Table 8 Thermal properties obtained from DSC analysis of HA, PVP and HA/PVP films

Thermal Properties	HA	PVP	HA/PVP7
T_g (°C)	158	157	150
ΔH_{relax} (J/g)	575.96	167.38	685.72

leads to a reduction in T_g, indicating a weakening of the intermolecular forces compared to neat HA. This behavior is associated with hydrogen bonding interactions between HA and PVP, which disrupt strong HA–HA interactions and restrict the formation of stable ordered domains. These observations are in good agreement with the FTIR results.

In terms of relaxation enthalpy, the HA/PVP7 film exhibits a higher value than the HA film. This increase may be attributed to the presence of more ordered regions within the HA/PVP7 film, as greater energy is required to overcome intermolecular interactions associated with such structural organization [45, 46]. Importantly, the T_g of the HA/PVP7 film (~150 °C) is lower than that of neat HA and remains well below its thermal degradation temperature (~220 °C), thereby reducing the risk of thermal degradation and facilitating processing via conventional thermal techniques such as extrusion or injection molding.

A weak exothermic event was observed during the cooling scan, which may be attributed to limited structural rearrangement in the amorphous phase, such as hydrogen-bond re-association and/or moisture-related reorganization, rather than pronounced crystallization [47].

3.9 Themal stability

The thermal degradation behavior of HA, PVP and HA/PVP films under a nitrogen atmosphere was investigated using TGA, as shown in Fig. 9 and summarized in Table 9. Both HA and PVP films exhibited two stages of degradation. The initial stage is attributed to the evaporation of moisture or weakly bound water within the films. During this stage, the PVP film showed a greater weight loss (16%) compared to HA (13%), reflecting the hydrophilic nature of PVP and its correlation with the high WVTR observed in the PVP film.

The second stage of degradation in the HA film was observed at 214 °C, with a maximum degradation rate (T_{max}) around 234 °C, corresponding to the dissociation of intermolecular bonds and partial breakdown of the polymer structure [47]. This stage proceeds with a char yield of approximately 32% at 600 °C. The relatively high char yield and broad thermal degradation range are attributed to the strong intermolecular interactions and high molecular weight of the HA used [47].

For PVP films, the second stage of thermal degradation begins at 335 °C, with a maximum degradation rate (T_{max}) observed at 430 °C, attributed to the breakdown of the PVP structure, particularly the degradation of carboxylate groups [48, 49]. PVP exhibits a higher degradation temperature than HA, indicating greater thermal stability. However, at 600 °C, the char yield of PVP is significantly lower (5%) compared to HA (32%), due to the formation of volatile decomposition products [50]. In contrast, HA decomposes into more stable residues, resulting in substantial char formation.

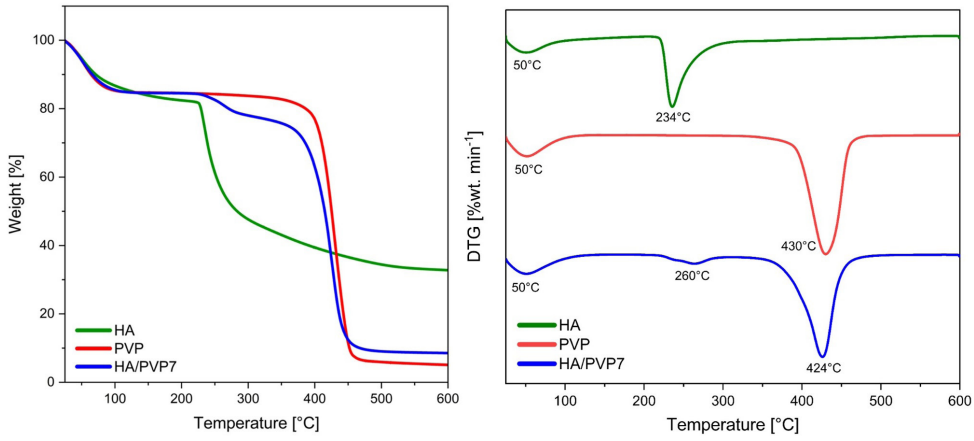

Fig. 9 TGA–DTG curves of HA, PVP and HA/PVP films

Table 9 Thermal degradation behavior of HA, PVP and HA/PVP films

Sample	First stage			Second stage			Third stage			
	T_0 [°C]	T_{max} [°C]	Mass loss [%]	T_0 [°C]	T_{max} [°C]	Mass loss [%]	T_0 [°C]	T_{max} [°C]	Mass loss [%]	Char yield [%]
HA	25	50	13	214	234	55	-	-	-	32
PVP	25	50	16	335	430	79	-	-	-	5
HA/PVP7	25	50	14	220	260	6	346	424	72	8

The thermal degradation of HA/PVP blend films occurs in three stages: (1) evaporation of moisture or weakly bound water, (2) degradation of the HA component, and (3) degradation of the PVP component. The increased weight loss during the first stage indicates that the addition of PVP raises the water content in the film due to its hydrophilic nature. The second stage of degradation occurs at a higher onset temperature (T_0 = 220 °C) and maximum degradation temperature (T_{max} = 260 °C) compared to the HA film, suggesting that the presence of PVP enhances the film's thermal stability. This shift to higher degradation temperatures is attributed to intermolecular interactions and good compatibility between HA and PVP. Furthermore, the crystalline structure induced by PVP may restrict polymer chain mobility, thereby increasing the energy required for thermal degradation. In the third stage, molecular interactions between HA and PVP also shift the degradation temperature of the PVP component. Regarding char yield, the incorporation of PVP results in a lower char yield due to reduced formation of carbonaceous residue during thermal decomposition.

4 Conclusion

This study investigated the physicochemical properties of HA and HA/PVP blend films. The HA/PVP 1:7 (w/w) blend film exhibited a more delicate and homogeneous morphology compared to pure HA and other HA/PVP compositions, indicating good miscibility between HA and PVP at this ratio. The incorporation of PVP into the HA increased the film's crystallinity; however, it also led to a reduction in hydrogen bonding and other secondary interactions. The mechanical properties of the blend films improved with increasing PVP content. Notably, the HA/PVP 1:7 (w/w) blend demonstrated mechanical performance comparable to that of PLA and PVA, with a tensile strength of 49.93 ± 9.34 MPa, elongation at break of 6.89 ± 0.31%, and an elastic modulus of 1.06 ± 0.24 GPa. The incorporation of PVP diminished the barrier performance of the films, as indicated by an increase in the water vapor transmission rate from 32.67 ± 1.11 $g \cdot m^{-2} \cdot h^{-1}$ for the HA film to 69.12 ± 1.14 $g \cdot m^{-2} \cdot h^{-1}$ for the HA/PVP 1:7 blend film, with both films still classified as exhibiting moderate barrier properties. However, contact angle measurements revealed that the addition of PVP led to a decrease in surface wettability. The HA/PVP 1:7 blend film (opacity = 0.73 1/mm) was slightly less transparent than the HA film (opacity = 0.70 1/mm). This blend also exhibited good thermal properties, with a glass transition temparature 150 °C and thermal stability up to 220 °C. The HA/PVP 1:7 (w/w) blend film, derived from environmentally friendly sources, may serve as a biodegradable material for packaging, polymer electrolyte membranes, or other potential applications.

Acknowledgement

The authors would like to express their sincere appreciation to the Ministry of Higher Education, Science, and Technology of the Republic of Indonesia for the financial support provided through the Fundamental Research Grant Scheme 2024. The authors also wish to thank the research laboratories at the Faculty of Science, Kasetsart University, for providing access to their facilities and resources.

References

[1] Zhao, X., You, F. "Decarbonizing energy: Plastic waste trade for zero waste 2040", Advances in Applied Energy, 17, 100216, 2025. https://doi.org/10.1016/j.adapen.2025.100216

[2] Stoett, P., Scrich, V. M., Elliff, C. I., Andrade, M. M., Grilli, N. D., Turra, A. "Global plastic pollution, sustainable development, and plastic justice", World Development, 184, 106756, 2024. https://doi.org/10.1016/j.worlddev.2024.106756

[3] Sheydaei, M. "Microplastics: Pollution of the modern world", Journal of Applied Material Science, 1, 210143, 2025. https://doi.org/10.22034/jams.2025.210143

[4] Carbery, M., O'Connor, W., Thavamani, P. "Trophic transfer of microplastics and mixed contaminants in the marine food web and implications for human health", Environment International, 115, pp. 400–409, 2018 https://doi.org/10.1016/j.envint.2018.03.007

[5] Lakhiar, I. A., Yan, H., Zhang, J., Wang, G., Deng, S., ..., Wang, X. "Plastic pollution in agriculture as a threat to food security, the ecosystem, and the environment: an overview", Agronomy, 14(3), 548, 2024. https://doi.org/10.3390/agronomy14030548

[6] Cordeiro, A., Hussain, M., Ramachandran, T., Beemkumar, N., Kumar, R., ..., Patil, A. Y. "Advancements in Packaging Materials: Trends, Sustainability, and Future Prospects", Circular Economy and Sustainability, 5(4), pp. 2959–2990, 2025. https://doi.org/10.1007/s43615-025-00586-4

[7] Graça, M. F. P., Miguel. S. P., Cabral, C. S. D., Correia, I. J. "Hyaluronic acid—based wound dressings: A review", Carbohydrate Polymers, 241, 116364, 2020. https://doi.org/10.1016/j.carbpol.2020.116364

[8] El-Aassar, M. R., El Fawal, G. F., Kamoun, E. A., Fouda, M. M. G. "Controlled drug release from cross-linked κ-carrageenan/hyaluronic acid membranes", International Journal of Biological Macromolecules, 77, pp. 322–329, 2015. https://doi.org/10.1016/j.ijbiomac.2015.03.055

[9] Kim, S., Cho D.-H., Kweon, D.-K., Jang, E.-H., Hong, J.-Y., Lim, S.-T. "Improvement of mechanical properties of orodispersible hyaluronic acid film by carboxymethyl cellulose addition", Food Science and Biotechnology, 29(9), pp. 1233–1239, 2020. https://doi.org/10.1007/s10068-020-00771-1

[10] Żołek-Tryznowska, Z., Kałuża, A. "The influence of starch origin on the properties of starch films: Packaging performance", Materials, 14(5), 1146, 2021. https://doi.org/10.3390/ma14051146

[11] Candido, I. C. M., Piovesan, L. F., Freire, A. L., Fotius, J. A. A., Isídio de Lima, J. J., Barud, H. S., de Oliveira, H. P. "Biodegradable hyaluronic acid-based triboelectric nanogenerator as self-powered temperature sensor", Materials Today Communications, 36, 106855, 2023. https://doi.org/10.1016/j.mtcomm.2023.106855

[12] Nešić, A., Ružić, J., Gordić, M., Ostojić, S., Micić, D., Onjia, A. "Pectin-polyvinylpyrrolidone films: A sustainable approach to the development of biobased packaging materials", Composites Part B: Engineering, 110, pp. 56–61, 2017. https://doi.org/10.1016/j.compositesb.2016.11.016

[13] Anwar, B., Nurhashiva, C., Arwa, W. R., Yuliani, G. "Physicochemical properties of bioplastic based on hydroxyethylcellulose and polyvinylpyrrolidone blend", The Journal of the Serbian Chemical Society, 89(2), pp. 215–230, 2024. https://doi.org/10.2298/JSC231023103A

[14] Unni, A., Mathew, M. M., Manathanath, M., Jacob, S., Sankaranarayanan, P., Vasu, S. T., Panicker, U. G. "Biocompatibility evaluation of nano-hydroxyapatite modified hydroxypropyl methylcellulose/polyvinylpyrrolidone blends", Polymer Bulletin, 81(4), pp. 3439–3458, 2024. https://doi.org/10.1007/s00289-023-04870-x

[15] Panzarasa, G., Osypova, A., Consolati, G., Pandini, S. "Microsegregating blends of ethyl cellulose and poly(vinyl pyrrolidone): A combined thermo-mechanical and positron annihilation spectroscopy study", Cellulose, 26(3), pp. 1619–1630, 2019. https://doi.org/10.1007/s10570-018-2220-6

[16] El Sayed, A. M., Mohamad, A. D. M. "Synthesis, structural, thermal, optical and dielectric properties of chitosan biopolymer: Influence of PVP and α-Fe_2O_3 nanorods", Journal of Polymer Research, 25(8), 175, 2018. https://doi.org/10.1007/s10965-018-1571-x

[17] Abou Taleb, M. H. "Thermal and spectroscopic studies of poly(N-vinyl pyrrolidone)/poly(vinyl alcohol) blend films", Journal of Applied Polymer Science, 114(2), pp. 1202–1207, 2009. https://doi.org/10.1002/app.30082

[18] Jeivan, A. O., Galus, S. "Edible pouch packaging for food applications – A review", Processes, 13(9), 2910, 2025. https://doi.org/10.3390/pr13092910

[19] Elakkiya, M., Revathy, M. S., Jansi, R., Janani, V. A., Kumar, A., Agrawal, A., Mishra, V. K., Shaaban, I. A., M. Hossain, M. K. "Investigation on structural and electrical properties of sodium alginate/PVP solid blend polymer electrolyte", Material Todays Communication, 42, 111067, 2025. https://doi.org/10.1016/j.mtcomm.2024.111067

[20] Shakeel, A., Gillani, S. E. H., Gill, Y. Q., Rasheed, M. H., Theravalappil. R., Younas, M., Mehmood, U. "Synergistic effects of polyvinylidene fluoride (PVDF) and polyvinylpyrrolidone (PVP) blends in gel electrolytes for efficient and long-term stability in dye-sensitized solar cells (DSSCs)", Journal of Physics and Chemistry of Solids, 192, 112087, 2024. https://doi.org/10.1016/j.jpcs.2024.112087

[21] Bhavsar, V., Tripathi, D. "*In vitro* biocompatibility study of microwave absorbing conducting polymer blend films for biomedical applications", Journal of Polymer Engineering, 41(7), pp. 565–575, 2021. https://doi.org/10.1515/polyeng-2020-0042

[22] Sionkowska, A., Gadomska, M., Musiał, K., Piątek, J. "Hyaluronic acid as a component of natural polymer blends for biomedical applications: A review", Molecules, 25(18), 4035, 2020. https://doi.org/10.3390/molecules25184035

[23] Alzain, H., Hussein, K., Jabr, I., Alsubaie, A. "Biodegradation of synthetic PVP biofilms using natural materials and nanoparticles", Green Processing and Synthesis, 12(1), 20230011, 2023. https://doi.org/10.1515/gps-2023-0011

[24] Birdibekova, A. V., Starostina, E. A., Kuryanova, A. S., Aksenova, N. A., Timashev, P. S., Akopova, T. A., Demina, T. S. "Layer-by-Layer Deposition of Chitosan/Hyaluronic Acid Polyelectrolyte Complex Coatings onto Polyester Films", Polymer Science, Series A, 65(6), pp. 672–681, 2023. https://doi.org/10.1134/S0965545X2460008X

[25] Lewandowska, K., Szulc, M. "Characterization of hyaluronic acid blends modified by poly(N-vinylpyrrolidone)", Molecules, 26(17), 5233, 2021. https://doi.org/10.3390/molecules26175233

[26] Pimentel, G. C., Sederholm, C. H. "Correlation of infrared stretching frequencies and hydrogen bond distances in crystals", The Journal of Chemical Physics, 24(4), pp. 639–641, 1956. https://doi.org/10.1063/1.1742588

[27] Anwar, B., Bundjali, B., Sunarya, Y., Arcana, I. M. "Properties of bacterial cellulose and its nanocrystalline obtained from pineapple peel waste juice", Fibers and Polymers, 22(5), pp. 1228–1236, 2021. https://doi.org/10.1007/s12221-021-0765-8

[28] Taher, N., Mantiri, D. M. H., Dien, H. A., Mentang, F., Montolalu, R. I., Ngangi, E. L. A. "Optimization and characterization of edible film composite of k-carrageenan Kappaphycus alvarezii and beeswax nanoemulsion", AACL Bioflux, 14(4), pp. 1897–1907, 2021. [online] Available at: https://bioflux.com.ro/docs/2021.1897-1907.pdf [Accessed: 19 August 2025]

[29] Wen, Y.-H., Tsou, C.-H., de Guzman, M. R.,Huang, D., Yu, Y.-Q., ..., Wang, Z.-H. "Antibacterial nanocomposite films of poly(vinyl alcohol) modified with zinc oxide-doped multiwalled carbon nanotubes as food packaging", Polymer Bulletin, 79(6), pp. 3847–3866, 2022. https://doi.org/10.1007/s00289-021-03666-1

[30] Tomoda, B. T., Yassue-Cordeiro, P. H., Ernesto, J. V., Santos Lopes, P., Oliveira Péres, L., Ferreira da Silva, C., Agostini de Moraes, M. "Characterization of biopolymer membranes and films: Physicochemical, mechanical, barrier, and biological properties", In: De Moraes, M. A., da Silva, C. F., Vieira, R. S. (eds.) Biopolymer membranes and films, Elsevier, 2020, pp. 67–95. ISBN 978-0-12-818134-8
https://doi.org/10.1016/B978-0-12-818134-8.00003-1

[31] Barroso, N., Guaresti, O., Pérez-Álvarez, L., Ruiz-Rubio, L., Gabilondo, N., Vilas-Vilela, J. L. "Self-healable hyaluronic acid/chitosan polyelectrolyte complex hydrogels and multilayers", European Polymer Journal, 120, 109268, 2019.
https://doi.org/10.1016/j.eurpolymj.2019.109268

[32] Kumar, R., Mishra, I., Kumar, G. "Synthesis and evaluation of mechanical property of chitosan/PVP blend through nanoindentation-A nanoscale study", Journal of Polymer and the Environment, 29(11), pp. 3770–3778, 2021.
https://doi.org/10.1007/s10924-021-02143-0

[33] Poornachary, S. K., Han, G., Kwek, J. W., Chow, P. S., Tan, R. B. H. "Crystallizing micronized particles of a poorly water-soluble active pharmaceutical ingredient: nucleation enhancement by polymeric additives", Crystal Growth & Design, 16(2), pp. 749–758, 2016.
https://doi.org/10.1021/acs.cgd.5b01343

[34] Liu, Y., Lv, X., Hu, X., Shan, Z.-H., Zhu, P.-X. "Effect of adding a small amount of high molecular weight polyacrylamide on properties of oxidized cassava starch", Carbohydrate Polymers, 81(4), pp. 911–918, 2010.
https://doi.org/10.1016/j.carbpol.2010.04.004

[35] Patil, S., Bharimalla, A. K., Mahapatra, A., Dhakane-Lad, J., Arputharaj, A., Kumar, M., Raja, A. S. M., Kambli, N. "Effect of polymer blending on mechanical and barrier properties of starch-polyvinyl alcohol based biodegradable composite films", Food Bioscience, 44, 101352, 2021.
https://doi.org/10.1016/j.fbio.2021.101352

[36] Cha, Y-C., Kim, E-T., Ahn, T-K., Choe, S. "Mechanical and morphological phase behavior in miscible polyethersulfone and polyimide blends", Polymer Journal, 26(11), pp. 1227–1235, 1994.
https://doi.org/10.1295/polymj.26.1227

[37] Gleadall, A. "Mechanical properties of biodegradable polymers for medical applications", In: Pan. J. (ed.) Modelling degradation of bioresorbable polymeric medical devices, Elsevier, 2015, pp. 163–199. ISBN 978-1-78242-016-3
https://doi.org/10.1533/9781782420255.2.163

[38] Vasi, A-M., Popa, M. I., Butnaru, M., Dodi, G., Verestiuc, L. "Chemical functionalization of hyaluronic acid for drug delivery applications", Material Science and Engineering: C, 38, pp. 177–185, 2014.
https://doi.org/10.1016/j.msec.2014.01.052 (23)

[39] Jambaladinni, S., Bhat, J. S. "The role of ZnO nanofillers in enhancing the properties of PVA/PVP blend nanocomposites", Iranian Journal of Science and Technology, Transaction A: Science, 45(5), pp. 1851–1860, 2021.
https://doi.org/10.1007/s40995-021-01177-2

[40] Sharma, D., Patel, N., Panjabi, S., Patel, V. "Structural, morphological, optical, and thermal properties of electrospun PbS/PVP-PEO nanofibers", Ceramics International, 49(6), pp. 8839–8846, 2023.
https://doi.org/10.1016/j.ceramint.2022.11.038

[41] Voronova, M., Rubleva, N., Kochkina, N., Afineevskii, A., Zakharov, A., Surov, O. "Preparation and characterization of polyvinylpyrrolidone/cellulose nanocrystals composites", Nanomaterials, 8(12), 1011, 2018.
https://doi.org/10.3390/nano8121011

[42] Huhtamäki, T., Tian, X., Korhonen, J. T., Ras, R. H. "Surface-wetting characterization using contact-angle measurements", Nature Protocols, 13(7), pp. 1521–1538, 2018.
https://doi.org/10.1038/s41596-018-0003-z

[43] Moreno-Ricardo, M. A., Gómez-Contreras, P., González-Delgado, A. D., Hernández-Fernández, J., Ortega-Toro, R. "Development of films based on chitosan, gelatin and collagen extracted from bocachico scales (Prochilodus magdalenae)", Heliyon, 10(3), e25194, 2024
https:/doi.org/10.1016/j.heliyon.2024.e25194

[44] Emblem, A. "Plastic properties for packaging materials", In: Emblem, A., Emblem, H. (eds) Packaging Technology: Fundamentals, Materials and Processes, Elsevier, 2012, pp. 287–309. ISBN 978-1-84569-665-8
https://doi.org/10.1533/9780857095701.2.287

[45] Gasperini, A., Wang, G.-J. N., Molina-Lopez, F., Wu, H.-C., Lopez, J., ..., Bao, Z. "Characterization of hydrogen bonding formation and breaking in semiconducting polymers under mechanical strain", Macromolecules, 52(6), pp. 2476–2486, 2019.
https://doi.org/10.1021/acs.macromol.9b00145

[46] He, Y., Zhu, B., Inoue, Y. "Hydrogen bonds in polymer blends", Progress in Polymer Science, 29(10), pp. 1021–1051, 2004.
https://doi.org/10.1016/j.progpolymsci.2004.07.002

[47] Lewandowska, K., Sionkowska, A., Grabska, S., Kaczmarek, B. "Surface and thermal properties of collagen/hyaluronic acid blends containing chitosan", International Journal of Biological Macromolecules, 92, pp. 371–376, 2016.
https://doi.org/10.1016/j.ijbiomac.2016.07.055

[48] Elashmawi, I. S., Elsayed, N. H. "The role of gold nanoparticles in the structural and electrical properties of Cs/PVP blend", Polymer Bulletin, 77(2), pp. 949–962, 2020.
https://doi.org/10.1007/s00289-019-02786-z

[49] Sreekanth, K., Siddaiah, T., Gopal, N. O., Jyothi, N. K., Kumar, K. V., Ramu, C. "Thermal, structural, optical and electrical conductivity studies of pure and Mn^{2+} doped PVP films", South African Journal of Chemical Engineering, 36, pp. 8–16, 2021.
https://doi.org/10.1016/j.sajce.2020.09.003

[50] Peniche, C., Zaldívar, D., Pazos, M., Páz, S., Bulay, A., San Román, J. "Study of the thermal degradation of poly(N-vinyl-2-pyrrolidone) by thermogravimetry–FTIR", Journal of Applied Polymer Science, 50(3), pp. 485–493, 1993.
https://doi.org/10.1002/APP.1993.070500312